INSTITUTE OF PHYSICS PUBLISHING NANOTECHNOLOGY
Nanotechnology **17** (2006) 5798–5804 doi:10.1088/0957-4484/17/23/015

Growth and characterization of self-assembled carbon nitride leaf-like nanostructures

Li Yang[1,4], Paul W May[1], Lei Yin[2], Tom B Scott[3], James A Smith[1] and Keith N Rosser[1]

[1] School of Chemistry, University of Bristol, Cantock's Close, Bristol BS8 1TS, UK
[2] Department of Aerospace Engineering, University of Bristol, Queen's Building, University Walk, Bristol BS8 1TR, UK
[3] Interface Analysis Centre, University of Bristol, Oldbury House, 121 St Michael's Hill, Bristol BS2 8BS, UK

E-mail: li.yang@bristol.ac.uk

Received 15 September 2006, in final form 11 October 2006
Published 16 November 2006
Online at stacks.iop.org/Nano/17/5798

Abstract
Carbon nitride nanostructures have been created using the novel technique of liquid phase pulsed laser ablation of a graphite target in ammonia solution. For ablation times between 1 and 7 h, 'leaf-shaped' nanostructures are formed by self-assembly of carbon nitride nanorods. With increasing ablation time, the crystallinity of the nanorod building blocks improves, and the length of the nanoleaf structures increases while the width remains constant. X-ray photoelectron spectroscopy results confirmed that nitrogen is chemically incorporated into the carbon network. The N–C (sp^2) bonding increases with increasing ablation time, whereas the N–C (sp) and N–C (sp^3) bonding behaviour is more complex. The optical properties for these leaf-like structures as a function of ablation time are also discussed.

(Some figures in this article are in colour only in the electronic version)

1. Introduction

Since the prediction by Liu and Cohen [1] in 1989 of a super-hard carbon nitride solid, extensive worldwide experimental and theoretical research efforts have been made to synthesize such a compound. According to theoretical predictions [1–3], C_3N_4 can adopt several different crystalline structures, including α-C_3N_4, β-C_3N_4, graphitic-C_3N_4 (g-C_3N_4), pseudocubic-C_3N_4 and cubic-C_3N_4. The most well-known form, β-C_3N_4, is based on the structure of β-Si_3N_4, with C substituted for Si. Since this compound would have low ionicity (∼7%) together with a short equilibrium volume bond length (∼1.47 Å), a high bulk modulus comparable to or even greater than that of diamond is expected. β-C_3N_4 was further predicted [1] to have a wide bandgap and high thermal conductivity, and hence may have potential applications as an electron emitter, variable-bandgap semiconductor and as a transparent hard coating [4]. As a result, the majority of reports of carbon nitride formation in the literature are for β-C_3N_4 [5, 6]. Less scientific attention has been given to the other structures of C_3N_4, despite calculations [2, 3, 7] predicting that α-C_3N_4 and g-C_3N_4 are more energetically stable (lower structural energy E_0) than β-C_3N_4, while both cubic- and pseudocubic-C_3N_4 are significantly higher in energy. There are only a few experimental reports of the successful synthesis of these phases, including evidence for the formation of α-C_3N_4 [8], g-C_3N_4 [9], or a mixture of phases [10].

Several methods of synthesizing carbon nitride have been reported, including radio frequency plasma deposition [11], pulsed laser ablation [12], ion-beam-assisted deposition [13], ion implantation [14] and magnetron sputtering [15]. Most experiments have yielded mainly amorphous CN_x films, although there are some reports of submicron quantities of crystalline material contained within the films [16–18]. Reports of C_3N_4 highly ordered structures are less common. The fact that there have been so few claims for crystalline C_3N_4 compounds highlights the difficulties in the synthesis of hard carbon nitrides due to their low thermodynamic

[4] Author to whom any correspondence should be addressed.

stability with respect to the elements (C and N). Nevertheless, Yin and co-workers [19] recently reported the synthesis of highly crystalline β-C_3N_4 nanorods using a combination of mechanically ground graphite nanoparticles and high-temperature chemical reaction. However, precise details of the deposition conditions have yet to be published.

We recently reported [20, 21] the successful nanoscale growth of crystalline carbon nitride using the novel method of liquid phase pulsed laser ablation (LP-PLA). This technique involves focusing a high-power laser beam onto the surface of a solid target (in our case graphite), which is submerged beneath a liquid. The interaction of the laser with the target causes the surface to vaporize in the form of an ablation plume, which contains species such as atoms, ions, and clusters, travelling with high kinetic energy. The species in the plume collide and react with molecules of the surrounding liquid, producing new compounds containing atoms from both the original target and the liquid. Due the intensity of the laser and the nanosecond timescales, the instantaneous temperatures and pressure within the reaction volume can be extreme (many thousands of K at tens of GPa) [22]. Such high-temperature, high-pressure, and high-density conditions provide a 'brute force' method of synthesizing novel materials that have hitherto been inaccessible using milder, more conventional techniques.

In our previous papers [20, 21], we gave the preliminary results for LP-PLA of graphite in ammonia solution, which yielded a large variety of carbon nitride nanostructures depending on the ablation conditions. We also presented some x-ray photoelectron spectroscopy (XPS), transmission electron microscopy (TEM) and Raman evidence which showed that the structures were probably composed of crystalline α- or β-C_3N_4. A mechanism was proposed whereby the ablation process first produced nanoparticles (∼10–20 nm diameter), which then elongated into one-dimensional nanorods with increased ablation time. The nanorods increased in length and began to coalesce into multi-layer structures. All these processes happened in a very short timescale due to the extreme energy conditions. After an ablation time of 1 h, these multi-layer structures self-assembled into distinctive two-dimensional structures which tapered to a point at each end, resembling the shape of a leaf. Further increases in ablation time increased the density of these leaf-like structures, until, at a certain critical concentration, they joined together into mesoscale loose networks. Finally, these networks self-assembled into micron-scale spiky 'flower-like' structures for ablation times above 12 h.

We now report a more detailed study of this process, concentrating on the time domain between 1 and 7 h where the leaf-like structures are formed. Results for the Raman spectra and optical properties (including Tauc bandgap) as a function of ablation time will be presented, as well as XPS analysis which shows the degree to which nitrogen can be incorporated into the C network.

2. Experimental section

2.1. General procedures

In a typical synthesis, a solid graphite target (diameter 16 mm by 4 mm height, Testbourne Ltd, 99.99%) was placed in a sealed stainless-steel cell at room temperature in a 5 ml solution of 35% ammonia solution (Fisher Scientific, used as received without further purification). The depth of the liquid above the graphite surface was ∼5 mm, which was thin enough to allow the laser to pass through and readily focus on the target without significant absorption, and also to confine the plume to a small volume. The laser used was the second harmonic of a Q-switched Nd:YAG (532 nm, pulse duration 15 ns) operating at 10 Hz, providing a fixed laser fluence of 100 mJ/pulse. The laser beam was directed by a prism and then focused using a 25 mm-focal-length lens through a quartz window in the top wall of the cell, then through the liquid layer to form a ∼0.5 mm-diameter spot on the surface of the graphite target. The cell was rotated at 700 rpm during ablation using a standard magnetic stirrer (8 mm × 1.5 mm) in order to reduce the effect of target ageing. The reactive ablation time was typically carried out for times of t = 1–12 h, after which a colloidal suspension of nanoparticles remained in the container. During ablation, the suspension changed from colourless to a pale brown, indicating an increase in solid product and/or a change in composition of the solid. The suspension was stable, with no precipitate being observed if the sample tube was left untouched for up to two months.

For subsequent analysis, samples of the suspension were pipetted onto a glass slide or TEM grid and allowed to dry in air. For some analysis techniques (in particular, Raman spectroscopy and XPS), the concentration of ablation products needed to be increased. This was achieved by evaporation of some of the liquid phase in the suspension in an oven in air. This concentrated suspension was then pipetted onto a glass slide and dried to produce a thin layer, as before. This pipetting and drying procedure was repeated many times to increase the thickness of the layer sufficient to obtain a high signal:noise ratio in the subsequent analysis.

2.2. Materials characterization

Transmission electron microscopy (TEM, using a JEOL 1200 EX operating at 120 kV) and selected area electron diffraction (SAED) were used to identify the structure and morphology of the materials that were prepared. High-resolution (HR) TEM was carried on a JEOL 2010 electron microscope at 200 kV. Laser Raman spectroscopy (Renishaw 2000, with an excitation of wavelength 325 nm) and XPS (Thermo VG Scientific) were performed *ex situ* to search for evidence of C–N, C=C and C≡N bonds. In order to ensure that the intense laser light was not damaging the carbon nitride structures, Raman spectra were taken at numerous locations on the sample, and repeated a number of times in the same location, to check that the spectra were unchanged. The XPS used Al Kα (1486.6 eV) radiation operating at 400 W (15 kV). High-resolution scans were acquired with a 30 eV pass energy and 200 ms dwell times. An ultraviolet–visible (UV–vis) spectrophotometer (Perkin Elmer Lamda 11) was used to monitor the changes in absorbance of the ablated solution, allowing the optical bandgap to be calculated.

3. Results and discussion

3.1. General structural features

TEM analysis revealed that the ablated product contained a range of unusual nanostructures depending upon ablation time,

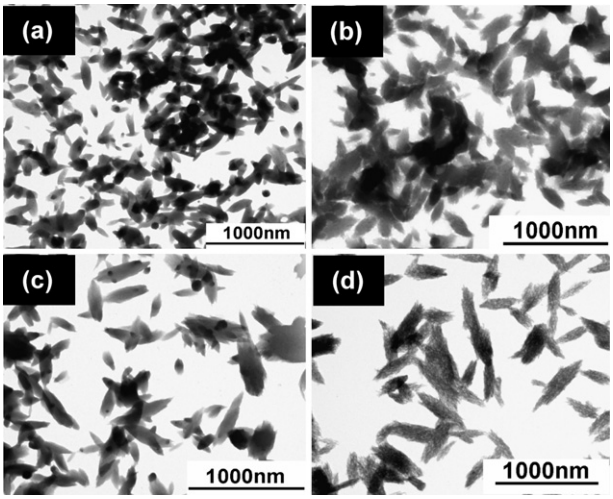

Figure 1. TEM images of as-synthesized C_3N_4 nanoleaf structures prepared using a laser fluence of 100 mJ per shot for ablation times of (a) $t = 1$ h, (b) 3 h, (c) 5 h and (d) 7 h. The concentration of the nanoleaf structures decreases with ablation time, but the average length of each nanoleaf increases.

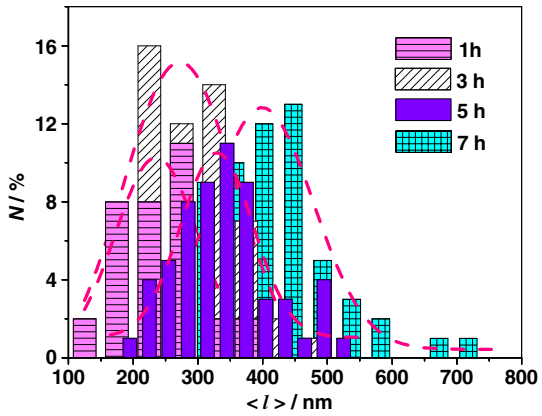

Figure 2. The corresponding nanoleaf length distribution for samples grown under different ablation times (with Gaussian fits to the data, dashed lines), as determined from TEM images. N = number fraction of nanoleaf structures, expressed as a percentage. Statistical analysis of the length of the C_3N_4 nanoleaf structures yields average lengths $\langle l \rangle$ of 235, 272, 336 and 399 nm for different ablation times $t = 1$, 3, 5, and 7 h, respectively.

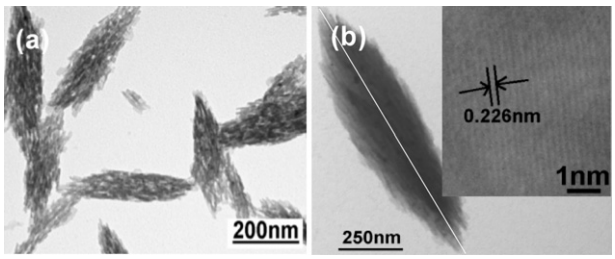

Figure 3. (a) High-magnification TEM image after 7 h ablation showing the carbon nitride nanoleaf structures. (b) A single leaf-like unit formed from numerous small nanorods. The inset is a HRTEM image recorded at the edge of the nanoleaf. The dotted line is showing the common direction along which all the component nanorods are aligned.

which are most likely formed as a result of self-organizing and close packing of the nanoparticles upon drying of the suspension. We previously described these nanostructures and proposed a mechanism for their formation [20]. Briefly, within a few minutes of the ablation process starting, spherical nanoparticles are created as a result of interaction between the high-energy plume and the liquid. With ablation times up to one hour, the concentration of the nanoparticles increased, and they began to join together along a common axis. The 'lined-up' particles fuse together into nanorods (width ∼10 nm, length ∼100–200 nm), which start to coalesce into multi-layered structures. For ablation times of 1–7 h, these structures self-organize into two-dimensional structures with both ends tapering to a point. These resemble the shape of a leaf, and so have been termed 'leaf-like' structures, as shown in figure 1. Statistical analysis of the length of the C_3N_4 nanoleaf structures (figure 1) yields average lengths $\langle l \rangle$ of 235, 272, 336 and 399 nm for different ablation times $t = 1$, 3, 5, and 7 h, respectively (figure 2), while the average widths remained roughly constant at 80 ± 20 nm. $\langle l \rangle$ increases in direct proportion to the ablation time until 7 h, at which time the structures begin to aggregate into larger units. For ablation times longer than 7 h, very few isolated nanoleaf structures are observed, with most being aggregated into disordered micron-scale complex crystallites in an open network. With ablation times >12 h, the nanoleaf structures coalesce to form the 'flower-like' structures that were mentioned in section 1 [20].

The high-magnification TEM image of a sample following 7 h ablation, shown in figure 3(a), indicates that these nanoleaf structures are themselves composed of a large number of smaller nanorods that have packed together in an ordered arrangement to form the leaf-like shapes. In particular, the image in figure 3(b), taken from a single nanoleaf, reflects the relationship between the orientation of the nanorods and the crystallography of the ordered nanoleaf array. The lattice fringes (figure 3(b), inset) give values of $d = 2.26 \pm 0.1$ Å for the (101) plane along the nanoleaf, which is consistent with crystalline β-C_3N_4 [23]. SAED analysis [20] also agrees with this, with the orientation of the nanoleaf being previously indexed as consistent with the $[1\bar{1}1]$ diffraction pattern of a hexagonal crystalline form of carbon nitride.

In this paper, we shall restrict ourselves to the time period 1 h $< t <$ 7 h, since it is in this time period that the process parameters are controlling the growth of the leaf-like structures. The influence of process conditions on the other morphologies that are created at longer or short ablation times will be presented elsewhere [24, 25].

3.2. Raman spectroscopy

Illustrative Raman spectra from the carbon nitride nanocrystallites at different ablation times are given in figure 4, showing broad features at ∼1600 and 1380 cm^{-1}. For amorphous carbon, graphite, or CN_x films, these features would correspond to the well-known G and D bands, respectively [26]. However, similar features would also be expected in the Raman spectra from the hexagonal lattices of both α- and β-C_3N_4 [27–29]. A wider scan range [21] shows a small peak at ∼2250 cm^{-1} assigned to C≡N, which is evidence for direct carbon–nitrogen

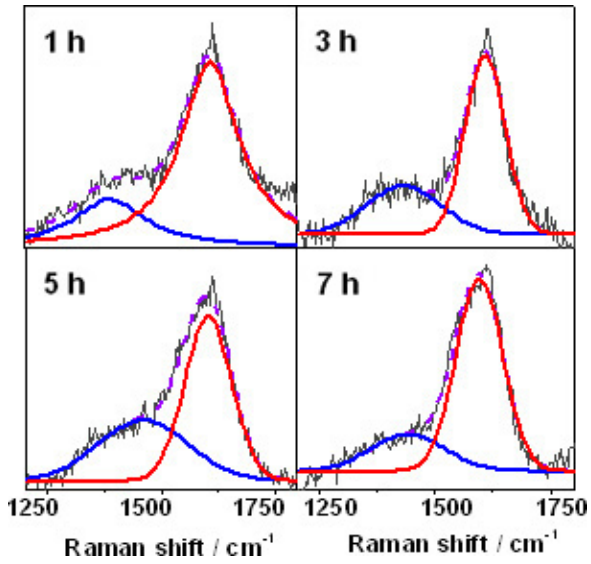

Figure 4. Raman spectra (325 nm excitation wavelength) from the C_3N_4 leaf-like structures following different ablation times at 100 mJ per shot laser fluence. The spectra are fitted in terms of two independent Gaussian functions (solid curves) centred ∼1600 cm^{-1} (‘*G* band’) and ∼1380 cm^{-1} (‘*D* band’), respectively, after subtracting a linear contribution for background fluorescence.

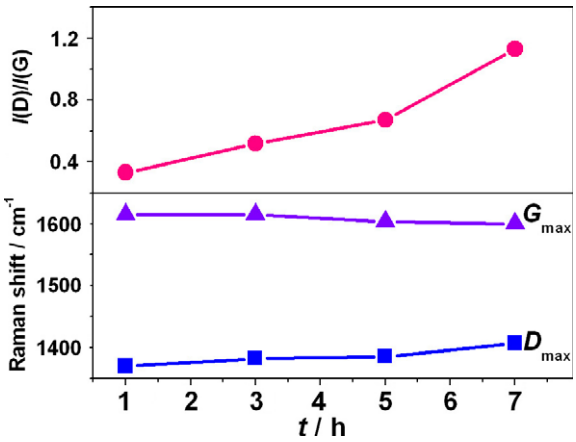

Figure 5. Plots showing the variation of G_{max}, D_{max} and $I(D)/I(G)$ as a function of ablation time, t, for the carbon nitride leaf-like nanocrystals synthesized by LP-PLA at 100 mJ per shot.

bonding in the system, although possibly as impurities rather than as part of the crystal lattice.

According to the empirical model for amorphous carbon proposed by Ferrari and Robertson [30], the wavenumbers of the *G* and *D* band maxima, G_{max} and D_{max}, and the ratio of their peak intensities, $I(D)/I(G)$, can be used to gain information about structure and disorder within such materials. Each spectrum was therefore deconvoluted using a Gaussian fit into the carbon nitride equivalents of graphitic *D* and *G* vibration modes.

G_{max}, D_{max} and $I(D)/I(G)$ as a function of ablation time are shown in figure 5. The $I(D)/I(G)$ ratio increases with increasing ablation time. This can probably be interpreted as an increase in the size of sp^2 clusters [31]. D_{max} is seen to shift to higher wavenumber as the ablation time is increased, while G_{max} decreases only slightly. The shift of the *D* band may indicate an increase in the number of carbon sp^3 bonds linking with N atoms [32]. This would result in an increase in the ratio of sp^3-to-sp^2 bonds [33], which is consistent with the production of C_3N_4. Lee *et al* [34] found that the G band for carbon materials shifts to higher energy (>1580 cm^{-1}) with improving crystalline quality, and to energies (<1575 cm^{-1}) for amorphous materials. The *G* band position for our samples does not change significantly with ablation time, indicating that the overall crystallinity of the samples remains constant. This is because the nanoleaf structures are not crystalline themselves, but are composed of an ordered arrangement of crystalline nanorods. Increasing the ablation time increases the number of nanorods in each nanoleaf, but does not change the crystallinity of the nanoleaf itself.

3.3. XPS analysis

X-ray photoelectron spectroscopy (XPS) measurements estimated that the overall elemental composition of the nanoleaf structures was 86.3% C, 11.4% N, and 2.3% O after 5 h, whereas for 7 h of ablation the values were 90.5% C, 7.8% N and 1.7% O. One possibility for the presence of the O signal is that the graphite target reacted directly with the water (or OH radicals generated in the water) during the high-temperature conditions in the ablation plume. However, since the O signal decreased with longer ablation time, this idea has been discounted. An alternative explanation is that prolonged exposure of the samples to the laboratory atmosphere led to possible contamination by absorbed or adsorbed water vapour. For pure C_3N_4, we would expect a composition of 42.8% C and 57.2% N, which shows that our samples are considerably carbon rich. Since we know from TEM observations that regions of the samples contain pure C_3N_4, we must conclude that our samples are a composite of crystalline C_3N_4 and an amorphous carbon background. This observation is consistent with the conclusions by other workers [35, 36], who found that it was difficult to generate highly ordered structures containing large concentrations of N incorporated into the C network.

The breadth and asymmetry of the C (1s) and N (1s) core-level XPS spectra shown in figure 6 indicate the presence of different bonding states within the crystallites. The core-level lines were fitted to a Gaussian function [37]. The N 1s feature is difficult to assign unambiguously, since it is known that N can give a broad XPS peak around 399 eV in some materials. Alternatively, a better fit can be achieved if the feature is deconvoluted into three peaks (as shown in figure 6), located at ∼398.5, ∼399.6 and ∼400.2 eV, respectively. The peaks situated at ∼398.5 eV can be assigned to sp^3 C–N bonds, and one at 400.2 eV assigned to sp^2 C=N bonds [38]. A peak centred at a binding energy ∼399.6 eV has been assigned by some groups [17, 39] to N atoms bonded to sp-hybridized C atoms (i.e. −C≡N). These assignments are also supported by *ab initio* binding-energy calculations [40]. Nevertheless, within experimental accuracy, it is impossible to distinguish between these two alternatives. Also, it should be noted that C≡N bonds can produce three peaks in this region [39]: 398.2 eV [41], 398.1 eV [42] and 400.1 eV [43]. However, these assignments have been discounted, since they are outside of the experimental accuracy of the XPS spectrometer. The

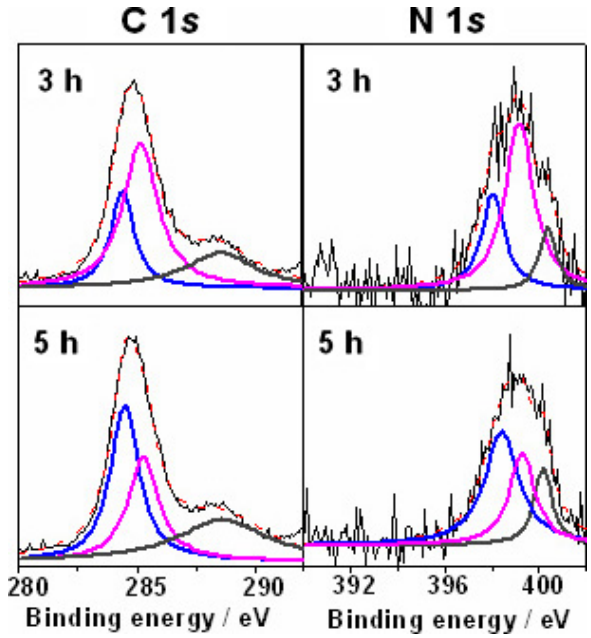

Figure 6. C (1s) and N (1s) XPS spectra of C_3N_4 nanostructures for different ablation times. Each spectrum has been deconvoluted by fitting to three Gaussian lineshape functions, with the total fitted line overlaid as a dashed line.

presence of sp^3 C–N in the ablated nanostructures is, again, in agreement with a C_3N_4 structure.

Similarly, the C 1s core-level spectra obtained by XPS (figure 6) was deconvoluted into three peaks located at ∼284.6, ∼285.5 and ∼288.5 eV, respectively. However, unlike nitrogen, verification of the assignment by independent C (1s) spectra was relatively difficult due to small shifts in binding energy and multiple bonding environments of the carbon. Carbon atoms may have zero, one, two, or three bonds with nitrogen atoms, which complicate the situation, so that there is a wide range of interpretation in the literature for carbon spectral feature identification. The peaks at ∼284.6 and ∼285.5 eV can be identified unambiguously as sp^2 and sp^3 hybridized carbon [44–46]. But the assignment for the peak at ∼288.5 eV has not yet reached a consensus. In our case, it is believed that this peak corresponds to N≡C sp bonding [43] supported by the Raman data [20]. Le Normand *et al* [47] have claimed that it is inappropriate to assign components appearing at higher energies to specific C–C or C–N bonding environments. After searching a comprehensive range of organic polymers, Beamson and Briggs [48] also found that no significant difference in C 1s position can be appreciated between sp^2 and sp^3-hybridized carbon bonded to nitrogen.

The relationship between ablation time and relative peak area fraction is shown in figure 7(a). The peak area corresponding to N=C (sp^2) bonding indicates a marked increase with prolonged ablation time, whereas the trends for C≡N (sp) and N–C (sp^3) are relatively complex. Nitrogen inclusion into the CN network changes the shape and position of the C 1s peak, as seen as in figure 7(b). However, only the signal attributed to C=C (sp^2) bonding shows smooth variation, i.e. increasing with ablation time, while all other signals show a more complicated trend.

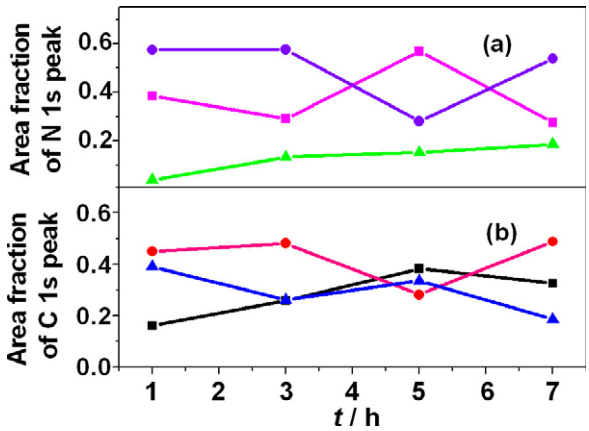

Figure 7. Plots showing the time dependences of the relative areas of the Gaussian functions used to fit (a) the N (1s) XPS peak (key: ■ 398.5 eV sp^3 C–N bonds, ● 399.6 eV C≡N bonds, ▲ 400.2 eV sp^2C=N bonds), and (b) the C (1s) XPS peak (key: ■ 284.6 eV, ● 285.5 eV, ▲ 288.5 eV).

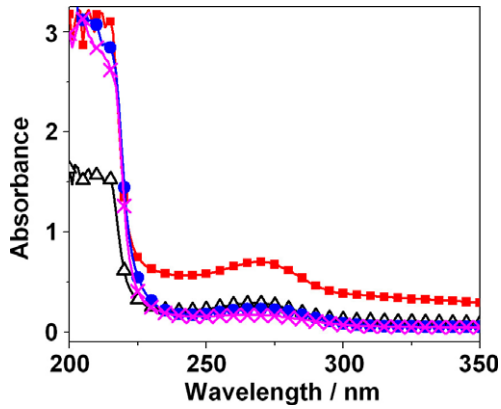

Figure 8. Plot of UV–visible absorbance from the ablation product (laser fluence at 100 mJ/pulse) for different ablation times, showing a prominent feature at ∼266 nm. Key: ■ 1 h, △ 3 h, ● 5 h, × 7 h.

3.4. Optical properties of the nanostructures

The UV–visible absorption spectra of the ablated solutions are shown in figure 8, displaying a feature at ∼266 nm. It is known [43] that the g- and α-C_3N_4 phases both contain aromatic 1,3,5-triazine rings, which exhibit absorption around 250 nm due to a π–π^* electronic transition. Hence, the experimental 266 nm absorption feature could indicate the presence of one or more of these phases of C_3N_4 within the ablated material. Interestingly, this feature is red-shifted with increasing nanocrystal size [49]. For example, the feature position changes from 266 to 269 nm for $t = 1$ h and $t = 5$ h, respectively. From figure 2, this corresponds to a mean length change from 235 to 336 nm.

Since carbon nitride is predicted to be semiconducting, the onset of absorption will give the optical (or Tauc) bandgap of the material, which can be found as the wavelength at which the extrapolation of the steeply rising part of the absorption spectrum crosses the wavelength axis. Using figure 8, we can estimate the threshold absorption wavelength and calculate a Tauc bandgap [50], which is shown as a function of ablation

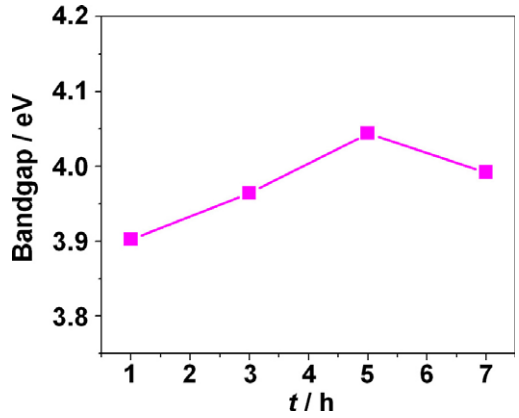

Figure 9. Time-dependent relationship of the calculated Tauc bandgap corresponding to different ablation times.

time in figure 9. The products had a calculated bandgap of around 3.9 ± 0.1 eV and compare favourably with the literature values for the predicted bandgap for α-C_3N_4 and β-C_3N_4 of 3.85 and 3.25 eV, respectively [3]. As can be seen in figure 9, the bandgap of the carbon nitride leaf-like structures held in solution increases smoothly with ablation time, e.g. from 3.90 eV after 1 h to 3.97 eV after 7 h. Notably, our C_3N_4 solution remained stable over two months with no sediment forming, thus these unique nanostructures having a tunable direct bandgap ∼4.0 eV might be materials that are suitable for optical applications.

4. Conclusions

Fabrication of well-organized carbon nitride leaf-like nanostructures can be achieved by LP-PLA using solid graphite and ammonia solution, without the assistance of any surfactants or pre-treatment. Evidence has been provided to illustrate that the nanostructured materials produced in this way are composed of crystalline α- or β-C_3N_4. Longer ablation times increased the length of the nanoleaf but did not significantly increase the width above a maximum value of 80 ± 20 nm. In addition, with increasing ablation time more nitrogen becomes incorporated into the structures, which improves the crystallinity of the component nanorods, but does not affect the crystallinity of the overall nanoleaf structures. The C_3N_4 nanostructures have a wide bandgap of ∼4.0 eV, which can be tuned over a small range (3.90–4.05 eV) by varying the ablation time, suggesting potential applications for the development of semiconductor or optical devices.

Acknowledgments

We thank Dr S A Davis, J Jones, C Archer and R Brown for their many and varied contributions to the work described herein. This research has been supported by Universities UK via the Overseas Research Scholarship (ORS) scheme, the University of Bristol and the School of Chemistry.

References

[1] Liu A Y and Cohen M L 1989 *Science* **245** 841
[2] Liu A Y and Wentzcovitch R M 1994 *Phys. Rev.* B **50** 10362
[3] Teter D M and Hemley R J 1996 *Science* **271** 53
[4] Wei J, Hing P and Mo Z Q 1999 *Surf. Interface Anal.* **28** 208
[5] Kundoo S, Banerjee A N, Saha P and Chattopadhyay K K 2003 *Mater. Lett.* **57** 2193
[6] Li Y, Xu S, Li H and Luo W J 1997 *Mater. Sci. Lett.* **17** 31
[7] Matar S F and Mattesini M 2001 *Chimie/Chemistry* **4** 255
[8] Malkow T 2000 *Mater. Sci. Eng.* A **292** 112
[9] Montigaud H, Tanguy B, Demazeau G, Alves I and Courjault S 2000 *J. Mater. Sci.* **35** 2547
[10] Fang P H 1995 *J. Mater. Sci. Lett.* **14** 536
[11] Kumar S, Butcher K S A and Tansley T L 1996 *J. Vac. Sci. Technol.* A **14** 2687
[12] Zocco A, Perrone A, D'Anna E, Leggieri G, Luches A, Klini A, Zergioti I and Fotakis C 1999 *Diamond Relat. Mater.* **8** 582
[13] Hammer P, Victoria N M and Alvarez F 2000 *J. Vac. Sci. Technol.* A **18** 2277
[14] Niu C M, Lu Y Z and Lieber C M 1993 *Science* **261** 334
[15] Lopez S, Dunlop H M, Benmalek M, Tourillon G, Wong M-S and Sproul W D 1998 *Surf. Interface Anal.* **25** 315
[16] Matsumoto S, Xie E Q and Izumi F 1999 *Diamond Relat. Mater.* **8** 1175
[17] Muhl S and Méndez J M 1999 *Diamond Relat. Mater.* **8** 1809
[18] Cao Y, Chen X, Lan Y, Li J, Xu Y and Xu T 2000 *Appl. Phys.* A **71** 465
[19] Yin W L, Bando Y, Li M S, Liu Y X and Qi Y X 2003 *Adv. Mater.* **15** 1840
[20] Yang L, May P W, Yin L, Brown R and Scott T B 2006 *Chem. Mater.* **18** 5058
[21] Yang L, Brown R, May P W and Yin L 2006 *Diamond Relat. Mater.* at press
[22] Wang J B, Zhang C Y, Zhong X L and Yang G W 2002 *Chem. Phys. Lett.* **361** 86
[23] Guo Y and Goddard W A III 1995 *Chem. Phys. Lett.* **237** 72
[24] Yang L, May P W, Yin L, Smith J A and Rosser K N 2006 *J. Nanopar. Res.* at press
[25] Yang L 2007 *PhD Thesis* University of Bristol UK in preparation
[26] Filik J 2005 *Spectrosc. Eur.* **17** 10
[27] Chowdhury A K M S, Cameron D C and Hashmi M S J 1998 *Thin Solid films* **332** 62
[28] Rodil S E, Ferrari A C, Robertson J and Milne W I 2001 *J. Appl. Phys.* **89** 5425
[29] Ferrari A C, Rodil S E and Robertson J 2003 *Phys. Rev.* B **67** 155306
[30] Ferrari A C and Robertson J 2000 *Phys. Rev.* B **61** 14095 and references therein
[31] Wang X C, Wu P, Li Z Q, Jiang E Y and Bai H L 2004 *J. Phys. D: Appl. Phys.* **37** 2127
[32] Chen C X, Chen W Z and Zhang Y F 2005 *Physica* E **28** 121
[33] György E, Mihailescu I N, Baleva M, Abrashev M, Trifonova E P, Szekeres A and Perrone A 2003 *Mater. Sci. Eng.* B **97** 251
[34] Lee E H, Hembree D M, Rao G R Jr and Mansur L K 1993 *Phys. Rev.* B **48** 15540
[35] Sjöström H, Staftröm S, Boman M and Sundgren J-E 1995 *Phys. Rev. Lett.* **75** 1336
[36] Terrones M *et al* 1999 *Adv. Mater.* **11** 655
[37] Doniach S and Sunjic M 1970 *J. Phys. C: Solid State Phys.* **3** 285
[38] Hellgren N, Johansson M P, Broitman E, Hultman L and Sundgren J-E 1999 *Phys. Rev.* B **59** 5162
[39] Hellgren N, Guo J, Såthe C, Agui A, Nordgren J, Luo Y, Ågren H and Sundgren J-E 2001 *Appl. Phys. Lett.* **79** 235416
[40] Souto S, Pickholz M, Santos M C D and Alvarez F 1998 *Phys. Rev.* B **57** 2536
[41] Ripalda J M, Montero I and Galan L 1998 *Diamond Relat. Mater.* **7** 402
[42] Ogata K, Chubaci J F D and Fujimoto F 1994 *J. Appl. Phys.* **76** 3791

[43] Khabashesku V N, Zimmerman J L and Margrave J L 2000 *Chem. Mater.* **12** 3264
[44] Javier D, Paoliceli G, Ferrer S and Comin F 1996 *Phys. Rev.* B **54** 8064
[45] Tabbal M, Merel P, Moisa S, Chaker M, Ricard A and Moisan M 1996 *Appl. Phys. Lett.* **69** 1698
[46] Angleraud B, Mubumbila N, Tessier P Y, Fernandez V and Turban G 2001 *Diamond Relat. Mater.* **10** 1142
[47] Le Normand F, Hommet J, Szörényi T, Fuchs C and Fogarassy E 2001 *Phys. Rev.* B **64** 235416
[48] Beamson G and Briggs D 1992 *High Resolution XPS of Organic Polymers* (Chichester: Wiley) p 182
[49] Jin R C, Cao Y W, Mirkin C A, Kelly K L, Schatz G C and Zheng J G 2001 *Science* **294** 1901
[50] Tauc J 1974 *Amorphous and Liquid Semiconductors* (New York: Plenum) p 171